ISSN 0015-4628, Fluid Dynamics, 2023, Vol. 58, No. 3, pp. 397–405. © The Author(s), 2023. This article is an open access publication.
Russian Text © The Author(s), 2023, published in Izvestiya RAN. Mekhanika Zhidkosti i Gaza, 2023, Vol. 58, No. 3, pp. 94–102.

Numerical Investigation of the Effect of Porous Wing Elements on the Properties of Supersonic Tip Vortices

A. E. Lutskii[a],* and A. V. Severin[a],**

[a] *Keldysh Institute of Applied Mathematics, Moscow, 125047 Russia*

* *e-mail: allutsky@yandex.ru*

** *e-mail: alsewerin@yandex.ru*

Received October 20, 2022; revised January 27, 2023; accepted January 28, 2023

Abstract—The effect of a porous wingtip on tip vortex formation and properties in a supersonic flow is studied. It is established that a porous wingtip has a considerable effect on the vortex structure and parameters reducing its intensity.

Keywords: tip vortex, vortex wake, supersonic flow, porous materials

DOI: 10.1134/S0015462823600360

An investigation of tip vortex formation and structure is an important problem of aerodynamics. The tip vortices are formed on outboard edges of wings and controls of flight vehicles (FV) due to the pressure difference. They exert influence on the aerodynamic characteristics of wings, the noise level, and the flight safety [1, 2]. The penetration of a FV or an element of its design into a tip vortex can lead to the loss of control or the breakdown. Different structural units, such as winglets, sharklets, and other types of wingtips [3], are used to reduce the tip vortices. The wingtips of subsonic FVs increase considerably the lift and reduce the drag. The possible application of the wingtips of the winglet type at supersonic velocities is investigated in [4] at $M = 1.62$. The authors of that study arrive at conclusion that in this flow regime the winglets are ineffective in reducing the wing drag.

One of the directions of perfecting the flight vehicle aerodynamics, which has been intensely developed most recently, is the use of structural units made of porous materials. The porous materials applied in flight vehicles can be produced basing on either various metals (nickel, bronze, etc.) or the materials based on heat-resisting porous carbon-based materials which possess high heat stability (2500 K) and a small specific density.

There has been much research devoted to the use of porous materials for stabilizing boundary layers [5–8], in bleed air-intake ducts [9], diffusers [10], nose cowls [11–13], and other structural units of flight vehicles.

For this reason, both the effect of porous design elements and tip vortices are of interest. The studies concerning this subject are few in number; we can mention, for example, the description of the NASA patent [14]. Some new and helpful effects can be found in this field. This study is devoted to the formation of tip vortices in the conditions, when either the entire wing or its part are made of a porous material. By way of illustration, we consider the straight wing of simple geometry in supersonic flow.

MATHEMATICAL MODEL AND NUMERICAL ALGORITHM

The calculations presented in this study were performed using the S3D program package [15] developed and implemented into software in the Keldysh Institute of Applied Mathematics. This program complex is intended for solving three-dimensional aerodynamic problems. An implicit difference scheme applied in this complex uses the LU SGS method for solving the system of linear equations. The fluxes on the cell faces are calculated using the Godunov interpolation scheme.

To describe flows of a perfect viscous compressible gas the system of unsteady Reynolds-averaged Navier–Stokes (URANS) equations with the one-equation Spalart–Allmaras (SA) turbulence model for compressible flows is used. The equations are discretized using the finite volume method which, as dis-

tinct from the finite difference method, can be applied to any geometry, operates with different grids, and makes it possible to avoid the problems with metric singularities of generalized coordinates.

The model of flow in a porous material is based on the restricted Baer–Nunziato model [16] which was primarily developed for describing the combustion and detonation processes in granular explosives. In this model, the medium is considered as a two-phase continuum that consists of the solid skeleton of unreacted explosive and the gas phase of combustion products. The model used in this study is a reduction of the Baer–Nunziato model based on the assumption that the solid skeleton remains fixed.

The instantaneous gas state is determined by its density ρ, the velocity vector u, and the pressure p. The gas is assumed to be a compressible, viscous, and heat-conducting medium. The skeleton is supposed to possess heat capacity and thermal conductivity, while the gas and skeleton temperatures are assumed to be the same.

It is assumed that the skeleton microstructure is isotropic and is characterized by the distribution of the skeleton volume fraction $\varphi = \varphi(\mathbf{x})$. The quantity $\alpha = \alpha(\mathbf{x}) = 1 - \varphi(\mathbf{x})$ is the local distribution of pores (porosity).

The geometric shape of a continuous solid body can be preassigned in two ways, namely, either letting $\alpha = 0$ or using the no-slip boundary conditions. In this study, the surfaces of continuous bodies are determined by the boundary conditions. Other-than-unity α values are used only in calculating the flows in porous regions of the wings.

As a result, we arrive at the following system of equations which describe in the continuum approximation compressible flows in the constrained environment of a porous permeable skeleton

$$\frac{\partial \alpha\rho}{\partial t} + \frac{\partial \alpha\rho u_k}{\partial x_k} = 0, \tag{1}$$

$$\frac{\partial \alpha\rho u_i}{\partial t} + \sum_{k=1}^{3}\frac{\partial \alpha(\rho u_i u_k + p\delta_{ik})}{\partial x_k} = p\frac{\partial \alpha}{\partial x_i} + \sum_{k=1}^{3}\frac{\partial \alpha\tau_{ik}}{\partial x_k} - g_i, \tag{2}$$

$$\frac{\partial \alpha\rho E}{\partial t} + \frac{\partial (1-\alpha) E_s}{\partial t} + \sum_{k=1}^{3}\frac{\partial \alpha\rho H u_k}{\partial x_k} = \sum_{k-1}^{3}\left(\frac{\partial \alpha\tau_{ik}u_i}{\partial x_k} - \frac{\partial \theta_k}{\partial x_k}\right). \tag{3}$$

Here, the notation is commonly accepted: $i, k = 1, 2, 3$ are the indices; ρ is the density, u_k are the velocity vector components, p is the pressure, $\tau_{ik} = 2\mu_{ef}e_{ik} - 2/3\mu_{ef}e_{jj}\delta_{ik}$ is the viscous stress tensor, $e_{ik} = 0.5(\nabla_i u_k + \nabla_k u_i)$ is the strain rate tensor, $\mu_{ef} = \mu_{mol} + \mu_{turb}$ is effective viscosity, $H = E + p/\rho$ is the total enthalpy, $E = E_t + W$ is the total energy of the gas phase, $E_t = p/[\rho(\gamma - 1)]$ is the internal energy per unit mass (determined by the equation of state for an ideal, calorically perfect gas), $W = 0.5\Sigma_{k=1}^{3}u_k^2$ is the kinetic energy per unit mass, $E_s = C_s T$ is the thermal energy of the skeleton, C_s is the heat capacity of the solid phase per unit volume, $\theta_k = -\lambda\nabla_k T$ is the molecular heat flux, λ is the thermal conductivity of the two-phase medium, T is the temperature, and δ_{ik} is the Kronecker tensor.

The molecular viscosity coefficient is assumed to be a function of the local air temperature T given by the semi-empirical Sutherland formula. The gas thermal-conductivity coefficient λ_g is related with the dynamic viscosity coefficient μ by the Prandtl number Pr which is assumed to be constant: Pr = 0.733. The thermal conductivity coefficient of the solid phase λ_s is assume to be constant and determined by material properties. The coefficient of thermal conductivity of the two-phase medium $\lambda = \alpha\lambda_g + (1 - \alpha)\lambda_s$.

The body force g_i in Eq. (2) is the viscous friction force that acts from the skeleton on the gas. It depends on the local velocity and the density of the gas and the skeleton microstructure (or the pore microstructure). Generally, the viscous friction force can be expressed in terms of the viscous drag coefficient in the Ergun form [17]

$$g_i = \frac{(1-\alpha) s_p C_d \rho |\mathbf{u}|}{8},$$

where $s_p = S_{elem}/V_{elem}$ is the skeleton dispersity, that is, the ratio of the interphase surface area to the skeleton volume per unit physical volume, and C_d is the drag coefficient determined by the empiric Ergun formulas as a function of the Reynilds number and the porosity.

A more detailed description of the numerical algorithms and mathematical models used in this study can be found in [18].

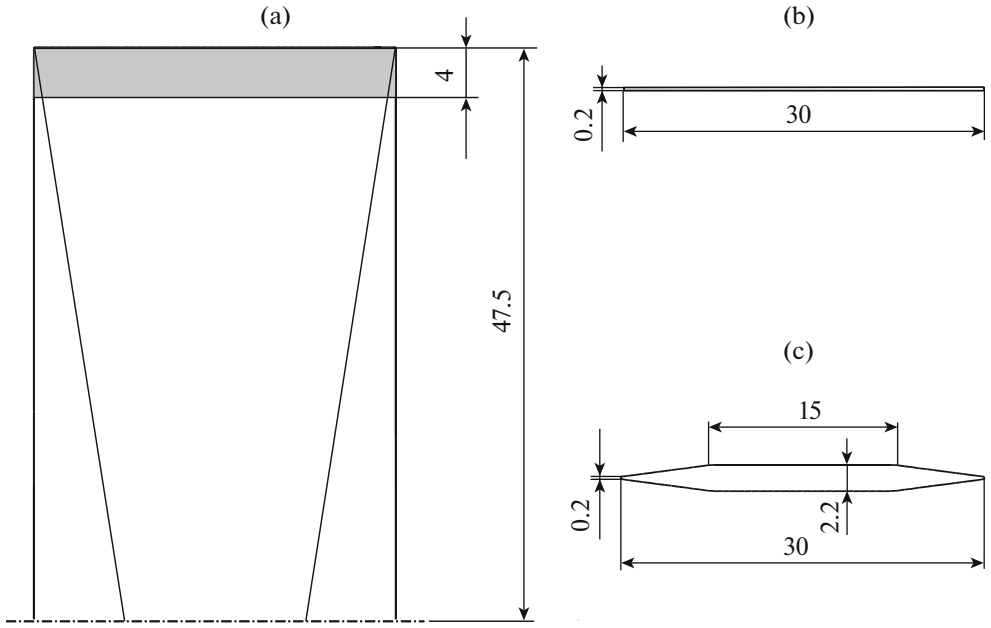

Fig. 1. Wing schematics: general view (a) and the airfoil near the edge (b) and the base (c).

The parallel algorithms of the numerical solution were realized in the multiprocessor K-100 system of the Keldysh Institute of Applied Mathematics [19].

NUMERICAL CALCULATIONS

The vortex wake in supersonic flow was investigated with reference to the example of a straight wing with 0.2 mm-thick leading and trailing edges. The wing chord and semi-span were 30 and 47.5 mm long, respectively. The wing airfoils near the base and on the outer edge are shown in Fig. 1. The wing shape between the given airfoils is such, that all the surfaces are plane, namely, a plane quadrangle in the mid-section and triangles near the leading and trailing edges. The wing schematics in plan are shown in Fig. 1.

The wing tip (cross-hatched in Fig. 1) is made of porous materials with different porosities, that is, volume fraction of the gas phase.

The porous material applied in the model is considered to be a continuous two-phase medium determined by two parameters, namely, porosity α, that is, the ratio of the gas phase volume to the overall volume, and the characteristic pore size interpreted as the mean diameter of the channels in the porous material.

The checking calculations were performed for a continuous wing and then the calculations for five porosity values were carried out: $\alpha = 0.4$, 0.6, 0.7, 0.8, and 0.9.

The characteristic pore size was taken to be 0.1 mm.

All the calculations were performed for the same oncoming flow with the Mach number $M = 3$, the Reynolds number based on 1 m $Re = 8\,803\,209$, and the angle of attack $\alpha = 10°$.

For the purpose of checking the grid convergence the calculations were performed on two grids.

The block-regular grid *1* consists of 5 951 600 cells with refinement near the wing surface, the leading and trailing edge, and the side edge. The cell thickness near the wing surface is 0.04 mm. The size of the region behind the wing is equal to nine chord lengths and that on wing exterior equals to the wing half-span. The no-slip condition is preassigned on the surface of the continuous wing portion and the interface between the continuous and porous surfaces. The mirror symmetry condition is preassigned in the $z = 0$ plane, where the wing base is mounted, the supersonic entry is assumed at the forward boundary of the domain, and the extrapolation condition is fulfilled on the other outer boundaries.

Grid *2* is also block-regular, with the cell number 7 312 800; near the leading and trailing edges the cell size in the longitudinal x direction is reduced by a factor of 10 compared with grid *1*, while that in the horizontal, transverse z direction is reduced by the factor of 1.5 near the side edge. The cell size in the y direction remains the same.

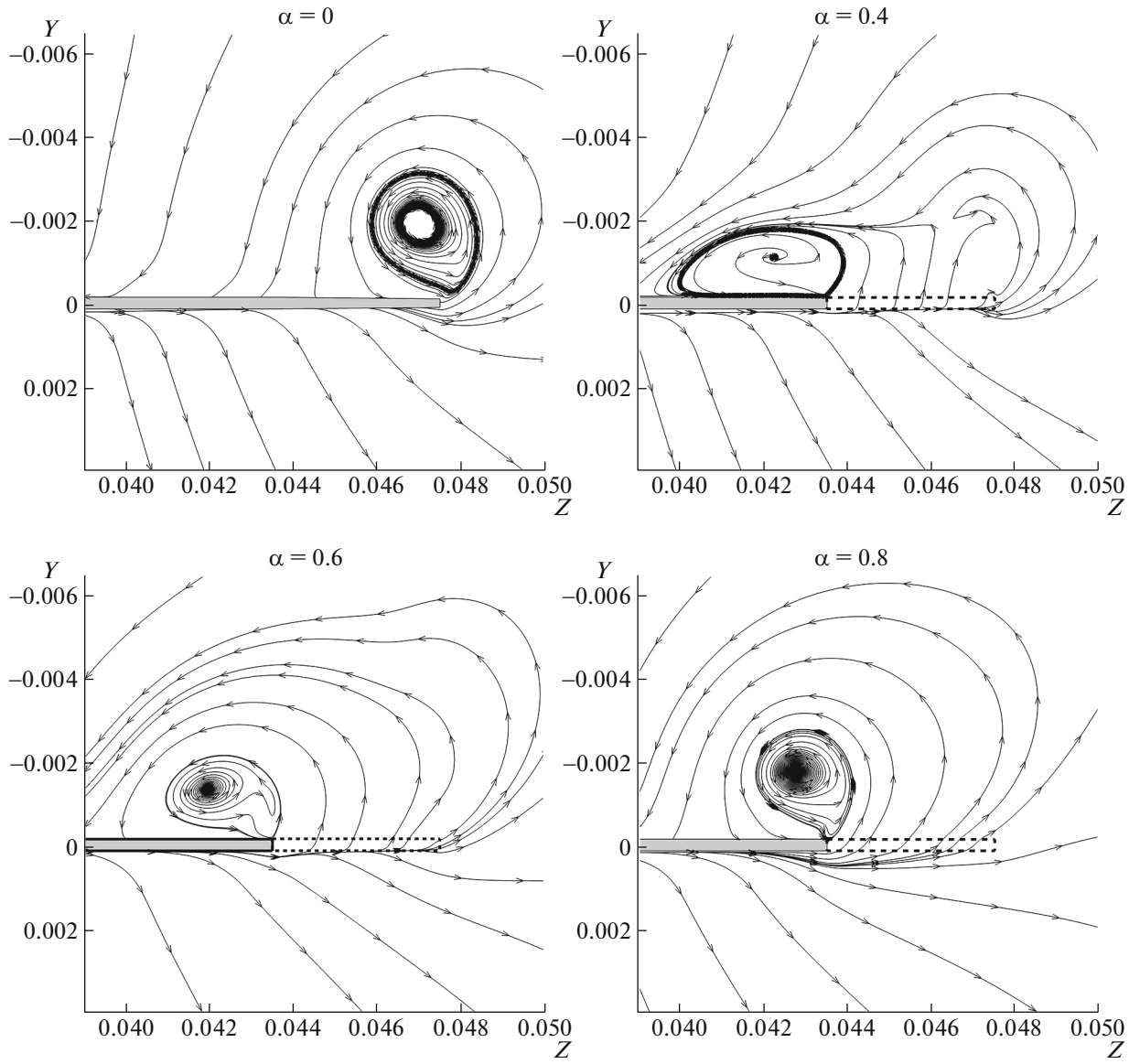

Fig. 2. Vector lines of the crossflow velocity field (u_z, u_y) in the plane of the $x = 0.0293$ section (trailing edge of the wing) for different values of the porosity α.

The origin of coordinates is in the plane of symmetry, near the leading edge of the wing. The x axis is directed downstream, the z axis is directed from the plane of symmetry to the wing edge, and the y axis is perpendicular to the flow and directed downward. The geometric dimensions are expressed in meters.

RESULTS OF THE CALCULATIONS

An analysis of the results of the numerical simulations showed that for all porosity values considered a tip vortex is formed. It is analogous to the vortex on a continuous wing but it is located near the end of the continuous region rather than in the vicinity of the edge of the porous wing tip. A circulation zone arises above the porous region of the wing but in all the cases the vortex center lies above the continuous region of the wing.

Since the air flowing from the wing undersurface passes now through the porous material, its velocity decreases, the vortex structure becomes complicated and nonsymmetric, and in most cases the vortex intensity is reduced. At large porosity values the vortex intensity may increase (Fig. 7).

Figure 2 presents the vortex structure in the transverse plane passing through the trailing edge of the wing for different porosity values and in the case of the control calculation for the continuous wing.

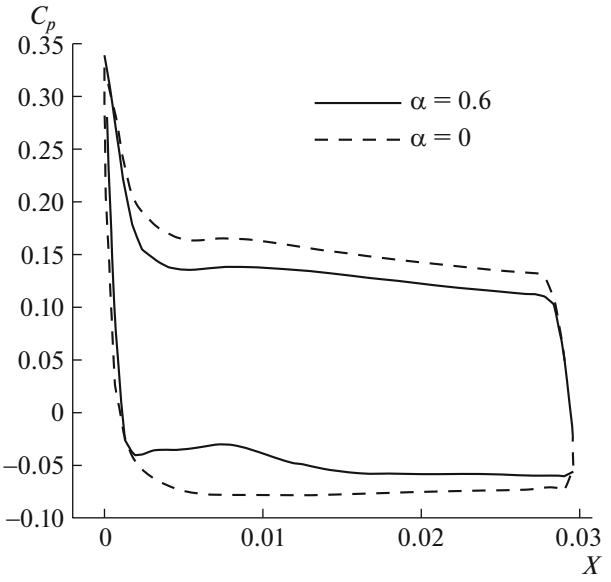

Fig. 3. Pressure coefficient on the wing surface $z = 0.042$.

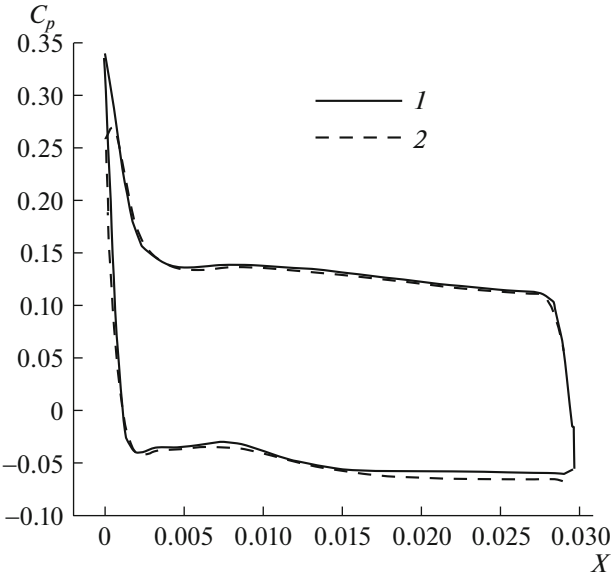

Fig. 4. Pressure coefficient calculated on the fine *1* and coarse *2* grids.

The vector lines of the crossflow velocity field (u_z, u_y) are presented. The porous region of the wing is encircled with a dash line.

It is interesting to note that at $\alpha = 0.8$ the vortex structure is qualitatively similar with that of the vortex on the continuous wing, only the vortex is displaced at a distance equal to the porous wingtip width. This means that the material with this porosity exerts a somewhat smaller effect on the flow structure and the wing is near-equivalent to a continuous wing of smaller span. However, some quantitative difference can be observable.

A variation in the vortex structure leads to a variation in the pressure distribution. In Fig. 3 the pressure coefficients are presented on the wing surface, in the $z = 0.042$ section for the continuous check-in wing and for $\alpha = 0.6$. Clearly that the pressure decreases on the wing undersurface and increases on the upper side.

In Fig. 4 the results of calculations on two grids are presented. Here, the pressure coefficients for $\alpha = 0.6$ calculated on grid *2*, the same as in Fig. 3, are compared with the results of calculations on grid *1*.

Table 1

Porosity	0	0.6	0.8	0.9
C_{xs}	0.3	0.292	0.294	0.295
C_{xp}	0.019	0.068	0.025	0.009
C_x	0.319	0.360	0.319	0.304
C_{ys}	1.263	1.22	1.228	1.229
C_{yp}	0.084	0.028	0.008	0.002
C_y	1.347	1.248	1.236	1.231
K	4.22	3.47	3.87	4.05

Clearly that there is a difference near the leading edge, where a shock is formed, but on the greater portion of the wing surface the discrepancy is small.

The pressure redistribution leads to a variation of the wing drag, lift, and lift-drag ratio. In Table 1 the aerodynamic coefficients (C_{xs}, C_{ys}) are presented for the wing midsection and the wing edge, which is porous for $\alpha \neq 0$. The drag of the continuous wing midsection consists of two components, namely, the pressure drag and the friction drag on the material surface. When a porous material is in flow, a third component is added to the two preceding. At small values of α the air flows over the material, the flow within the material is only slight, and, therefore, the third component is small. At large α a considerable portion of the air passes through the material but the internal friction drag is small due to a great number of air voids in the material. The greatest drag must be observable at medium values of α, and we can see that at $\alpha = 0.6$ it is actually higher than for the other values.

The differences in the vortex structure and intensity are conserved in the process of its downstream evolution. In Fig. 5 the longitudinal vorticity $\Omega_x = \partial u_z/dy - \partial u_y/dz$ and the Mach number at the center of the vortex are presented for the continuous wing and for $\alpha = 0.6$.

The Mach number at the vortex axis is considerably smaller in the case of the porous wingtip. In this case, the difference in the gas velocity is slight, while the speed of sound and the pressure turn out to be greater.

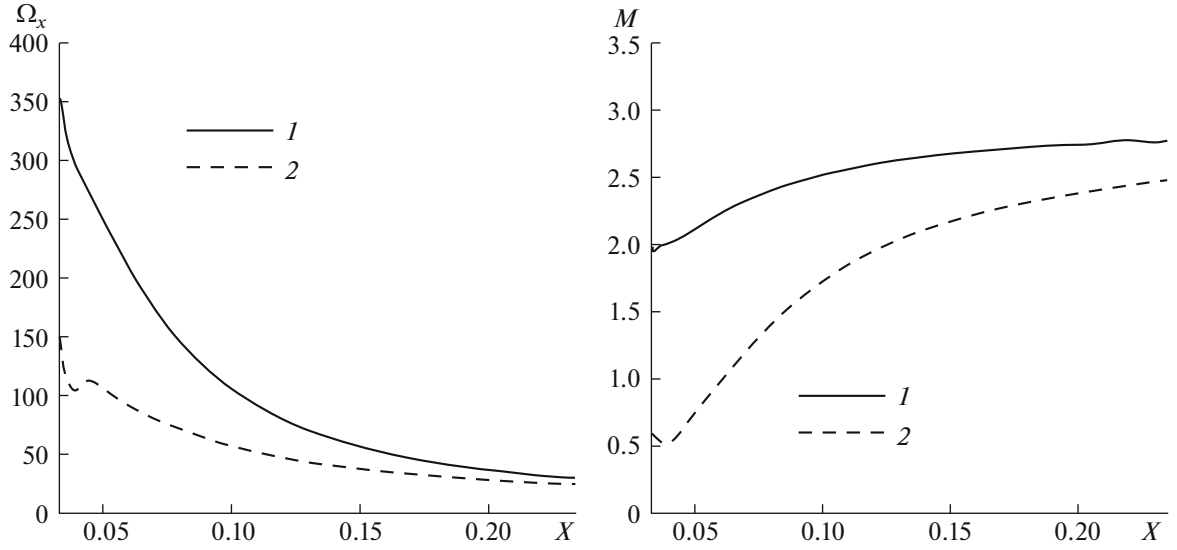

Fig. 5. Longitudinal vorticity (Ω_x,10^3 s^{-1}) and Mach number (M) at the vortex center for the porous *1* and continuous *2* wings.

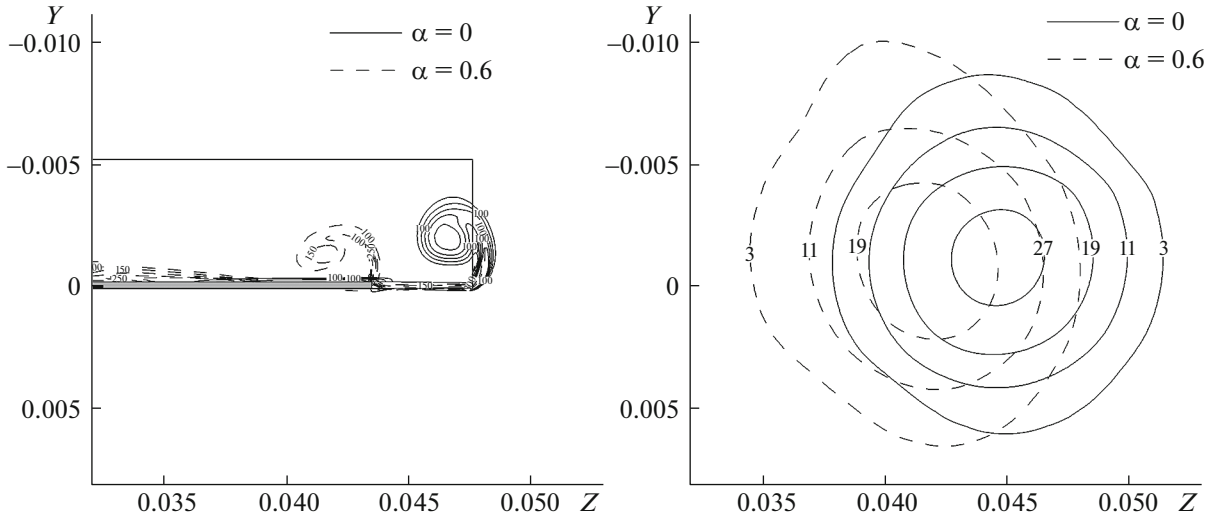

Fig. 6. Contours of the longitudinal vorticity (10^3 s^{-1}) in the sections $x = 0.0293$ (left) and $x = 0.2348$ (right).

In Fig. 6 we have plotted the isolines of longitudinal vorticity in the section $x = 0.2348$ (6.85 chord lengths from the trailing edge) behind the continuous wing (continuous curves) and the wing provided with a porous tip with the porosity $\alpha = 0.6$ (dashed curves). For the sake of clarity the contours of the wing and its trailing edge are also presented in the figure. The porous wingtip is covered with gray. Clearly that the vorticity is considerably reduced (its maximum has become 23.9 rather than 29.7), while the center of the vortex has displaced from the edge toward the boundary between the continuous and porous parts of the wing.

In Fig. 7 the flow parameters are presented, namely, the longitudinal vorticity Ω_x and the tangential Mach number M_{yz} along the line passing through the vortex center, perpendicular to its axis. The sections $x = 0.1348$ (at a distance of 3.5 chord lengths behind the edge) and $x = 0.2348$ (6.85 chord lengths) are presented. The curves are plotted for the continuous wing ($\alpha = 0$) and three porosity values $\alpha = 0.4$, 0.6, and 0.8.

Despite the fact that the vortex centers on the continuous wing ($\alpha = 0$) and the wing with a porous tip are at different points in the z coordinate, it can be seen in Fig. 7 that in all the cases the vortex center positions in the y coordinate are similar in value. It is interesting to note that the vortex structures on the continuous and $\alpha = 0.8$ wings are very similar and differ from each other considerably less than on the wing with other porosity values. This indicates that the wingtip with a high porosity has only a small effect on the vortex and this wing is near-equivalent with a smooth wing having a smaller span.

SUMMARY

The results of the numerical investigation of a tip vortex in supersonic $M = 3$ flow are presented for a wing with the wingtip made of a porous material at different porosity values. In the calculations the mathematical model of gas flow through a porous medium, the algorithms of turbulent flow modeling, and their parallel realization on multiprocessor computational systems were used.

The numerical results obtained show that a tip vortex formed on the wing with a porous tip is similar with that formed on a continuous wing. However, the vortex parameters, structure, and location differ considerably. In all the cases considered the vortex is formed near the edge of the continuous portion of the wing rather than near the boundary of the porous material.

When the porosity value is smaller than 0.8, the vortex becomes less intense; at the porosities 0.8 and 0.9 the vortex strength increases somewhat. The wing drag and lift decrease. Thus, there arises a possibility of controlling the vortex generation process.

The calculations are performed for the model wing with a simple geometry. They demonstrate the possibility in principle to control the tip vortex parameters using porous wingtips. In the case of other wing

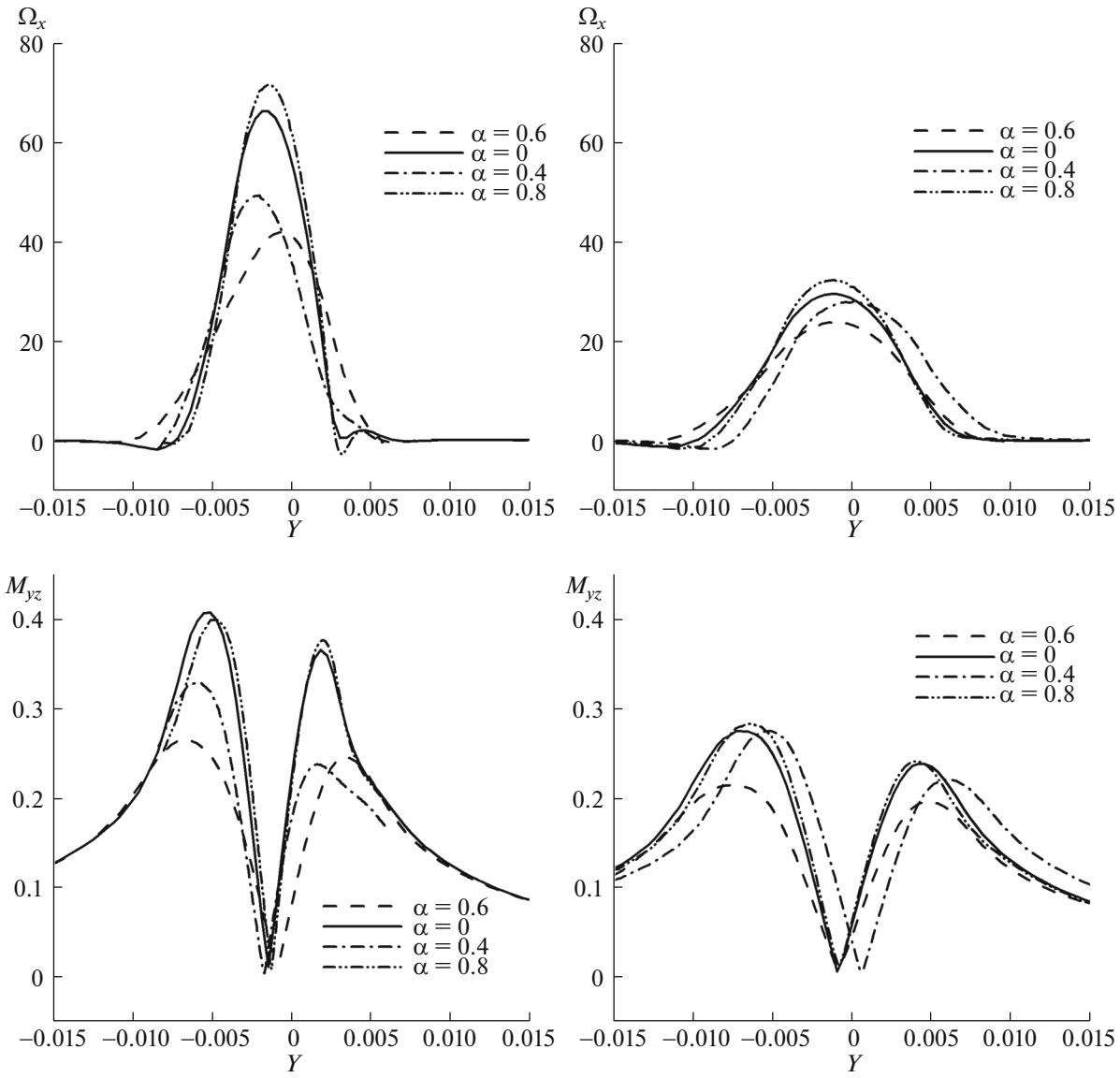

Fig. 7. Longitudinal vorticity Ω_x and tangential Mach number M_{yz} in the sections $x = 0.1348$ and 0.2348.

geometries the effects can be different. An analogous problem for a delta wing is of interest and can be subject of further studies.

FUNDING

The study is carried out with the financial support of the Russian Scientific Foundation (project no. 22-21-00470).

CONFLICT OF INTEREST

The authors declare that they have no conflicts of interest.

REFERENCES

1. Ginevskii, A.S. and Zhelannikov, A.I., *Vikhrevye sledy samoletov* (Vortex Wakes of Aircraft), Moscow: Fizmatlit, 2008.
2. Vyshinskii, V.V. and Sudakov, G.G., Vortex wakes of aircraft and the issues of flight safety, *Trudy MFTI*, 2009, no. 1(3), pp. 73–93.
3. Whitcomb, R.T., A design approach and selected wind-tunnel results at high subsonic speeds for wing-tip mounted winglets, *NASA-TN-D-8260*, 1976.
4. Keenan, J.A. and Kuhlman, J.M., The effects of winglets on low aspect ratio wings at supersonic Mach numbers, *NASA Contractor Report* 4407.
5. Kornilov, V.I. and Boiko, A.V., Experimental modeling of air blowing into a turbulent boundary layer using an external pressure, *Techn. Phys.*, 2016, vol. 61, no. 10, pp. 1480–1488.
6. Lysenko, V.I., Smorodskii, B.V., Ermolaev, Yu.G., Gaponov, S.A., Kosinov, A.D., Semenov, N.V., and Yatskikh, A.A., Effect of heavy gas injection into the wall layer of a supersonic boundary layer on its transition, *Sibir. Fiz. Zh.*, 2017, vol. 12, no. 1, pp. 50–56.
7. Tsiberkin, K.B., On the structure of the steady-state flow velocity field near the interface between a homogeneous liquid and Brinkman porous medium, *Techn. Phys.*, 2016, vol. 61, no.8, pp. 1181–1186.
8. Shiplyuk, A.N., Burov, E.V., Maslov, A.A., and Fomin, V.M., Effect of porous coatings on stability of hypersonic boundary layers, *J. Appl. Mekh. Tekhn. Phys.*, 2004, vol. 45, no. 2, pp. 286–291.
9. Fomin, V.M., Zapryagaev, V.I., Lokotko, A.V., Volkov, V.F., Lutskii, A.E., Men'shov, I.S., Maksimov, Yu.M., and Kirdyashkin, A.I., Aerodynamic characteristics of a body of revolution with gas-permeable surface areas, *J. Appl. Mekh. Tekhn. Phys.*, 2010, vol. 51, no. 1, pp. 65–73.
10. Willis, B.P., Davis, D.O., and Hingst, W.R., Flowfield measurements in a normal-hole-bled oblique shock-wave and turbulent boundary-layer interaction, *AIAA Paper* no. 2885, 1995.
11. Poplavskaya, T.V., Kirilovskiy, S.V., and Mironov, S.G., Supersonic flow around a cylinder with front gas-permeable insert which modeled by skeleton of porous material, *AIP Conf. Proc.*, 2016, vol. 1770, 030067.
12. Schuelein, E., Shock-wave control by permeable wake generators, *5th Flow Control Conf., Fluid Dynamics and Co-located Conferences*, Chicago, Illinois, 28 June–1 July, 2010.
13. Fomin, V.M., Mironov, S.G., and Serdyuk, K.M., Reducing the wave drag of bodies in supersonic porous materials, *Techn. Phys. Lett.*, 2009, vol. 35, no. 2, pp. 117–119.
14. *Winglet with injected flow*. https://technology.nasa.gov/contact-us/TOP2-289
15. Men'shov, I.S. and Severin, A.V., Program complex S3D. https://cfd.imamod.ru/FILES/2015/2015_CFD-Weekend_Abstracts.pdf
16. Baer, M.R. and Nunziato, J.W., A two-phase mixture theory for the deflagration-to-detonation transition (DDT) in reactive granular materials, *Int. J. Multiphase Flow*, 1986, no. 12, pp. 861–889.
17. Ergun, S., Fluid flow through packed columns, *Chem. Eng. Prog.*, 1952, vol. 48.
18. Severin, A.V., Lutskii, A.E., and Men'shov, I.S., High-speed channel flow control with porous inserts, *Math. Model. Computer Simulation,* 2022, vol. 34, no. 6, pp. 937–945.
19. Computation Complexes MVS-Express, K-100, and K-600 of the Institute of Applied Mathematics of the Russian Academy of Sciences. http://www.kiam.ru

Translated by M.Lebedev